$La_{48}Br_{81}Os_8$: Isolated Clusters in an Unusual Superstructure with Significantly Greater Intercluster Bonding

Seung-Tae Hong, Laura M. Hoistad, and John D. Corbett*

Department of Chemistry, Iowa State University, Ames, Iowa 50011

Received June 15, 1999

Exploration of reactions in the La−Br−Z system for Z = Fe, Ru, and Os in welded Nb containers at 900−950 °C resulted in only the title phase. The $La_{48}Br_{81}Os_8$ stoichiometry is very close to that of known triclinic $Pr_6Br_{10}Os$ but with an ∼32-times larger cell, 138 independent atoms, and completely different intercluster connectivities in a complex monoclinic superstructure (a = 33.076(5) Å, b = 23.466(3) Å, c = 23.537(2) Å, β = 110.701(4)°, $P2_1/c$ (No. 14), Z = 4, 23 °C). Tetragonally compressed, ∼16 e^- lanthanum octahedra centered by Os are heavily interbridged by Br, including Br^{f-a} (f = face) and Br^{i-a-a} functions, to increase coordination numbers about some Br (to 4) and La (to 6) and to give an average of 19.63 bonded Br/La_6Os vs the usual 18. These result in a cell volume 10% less than for an equivalent (hypothetical) $La_6Br_{10}Os$ and Br−Br contacts as short as 3.30 Å. Increased polar La−Br interactions presumably drive these changes. Optimal atom sizes for this structure have been found so far only in this novel compound.

Introduction

Exploratory synthesis in the search for new compounds, structures, and properties is an important aspect of materials chemistry, leading to the production of a large variety of new phases, sometimes unprecedented or unforeseen. The forecast of phase stability even among a collection of clear alternatives remains one of the great challenges in solid-state science, where the undiscovered possibilities sometimes seem to present almost overwhelming barriers to success. On the other hand, this lack of predictability can offer great excitement and surprise with the discovery of unknown, even unparalleled compounds.

A unique field of solid-state chemistry has been developed for the cluster halides of the first two transition-metal groups, namely for the Zr, Hf (Ti, Th), and the rare-earth element R (Sc, Y, and La plus the lanthanides Ce−Lu) families with halide X = Cl, Br, and I.[1−3] The nominally octahedral metal clusters present in all of these are evidently stable only when centered by one of a sizable variety of interstitial heteroelements Z. The typical cluster is usually isolated and insulated from its environment by 12 edge-bridging halogen atoms (X^i) plus, commonly, additional outer halide atoms X^a that bond to, and often bridge between, metal vertices, viz., $R_6(Z)X^i_{12}X^a_n$. This simple classification excludes some more complicated bridging functions. The rare-earth elements provide a virtually distinctive cluster chemistry compared with that for zirconium and hafnium, doubtlessly because of the reduced number of metal valence electrons. For these, only three ternary structure types have been reported that contain isolated clusters, while the remainder of the reduced halides (X:R ≤ 1.43:1) exhibit cluster condensation, usually through shared edges, to form oligomers, chains, or double-metal-layered phases, depending principally upon the X:R ratio. Different structures found for a given ratio further depend on the connectivities provided by the halide atoms as these interlink the clusters into different frameworks.

The three types of discrete ternary cluster structures for these elements are $R_7X_{12}Z$, $R_6X_{10}Z$, and $R_{12}X_{17}Z_2$. The rhombohedral $R_7X_{12}Z$ structure is derived from that of $Zr_6X_{12}Z$ by insertion of a seventh oxidized (R^{III}) atom in the antiprismatic cavity that lies midway between clusters along the $\bar{3}$ axis (z).[4−7] The second type with $Y_6I_{10}Ru$ as the parent structure[8] achieves a reduced halogen content by means of X^{i-i} atoms that bridge edges on pairs of adjoining clusters into chains. Systematic syntheses of $R_6I_{10}Z$ and $R_7X_{12}Z$ phases for R = Y, Pr, and Gd and a large range of Z[7] and of $Pr_6Br_{10}Z$[9] with Co, Ru, and Os show how frequently this type structures occurs and how widely the cluster electron count (16−22) may vary from the optimal 18. The third structure type has been found for triclinic $Pr_{12}I_{17}Fe_2$, $Pr_{12}I_{17}Re_2$,[10] $La_{12}I_{17}Fe_2$, and $Ce_{12}I_{17}Mn_2$.[11] This unusually low I:R ratio with only isolated clusters is achieved in a relatively complex structure by means of seven I^{i-i} bridges per cluster as well as one novel I^{i-a-a} mode.

Many of the structural novelties occur with iodides, while chlorides are relatively sparse in new chemistry. Reduced bromides are generally less well studied. The Pr−Br−Z systems yielded a variety of structural types: triclinic $Pr_6Br_{10}Z$ for Z = Co, Ru, and Os as well as the monoclinic Pr_3Br_3Ru and several cubic Pr_3Br_3Z[9] with condensed (metal edge sharing) clusters. Recent investigations on the Sc−Br and Y−Br systems have also provided oligomeric (tetrameric) condensed cluster compounds $R_{16}Br_{20}Z_4$ (R = Sc, Z = Fe, Os; R = Y for Z = Ru),

(1) Ziebarth, R. P.; Corbett, J. D. *Acc. Chem. Res.* **1989**, *22*, 256.
(2) Simon, A.; Mattausch, Hj.; Miller, G. J.; Bauhofer, W.; Kremer, R. K. In *Handbook on the Physics and Chemistry of Rare Earth*; Gschneidner, K. A., Eyring, L., Eds.; Elsevier Science Publishers: Amsterdam, 1991; Vol. 15, p 191.
(3) Corbett, J. D. In *Modern Perspectives in Inorganic Crystal Chemistry*; Parthé, E., Ed.; Kluwer Academic Press: Dordrecht, The Netherlands, 1992; pp 27−56.
(4) Hwu, S.-J.; Corbett, J. D. *J. Solid State Chem.* **1986**, *64*, 331.
(5) Dudis, D. S.; Corbett, J. D.; Hwu, S.-J. *Inorg. Chem.* **1986**, *25*, 3434.
(6) Hughbanks, T.; Corbett, J. D. *Inorg. Chem.* **1988**, *27*, 2022.
(7) Payne, M. W.; Corbett, J. D. *Inorg. Chem.* **1990**, *29*, 2246.
(8) Hughbanks, T.; Corbett, J. D. *Inorg. Chem.* **1989**, *28*, 631.
(9) Llusar, R.; Corbett, J. D. *Inorg. Chem.* **1994**, *33*, 849.
(10) Park, Y.; Corbett, J. D. *Inorg. Chem.* **1994**, *33*, 1705.
(11) Lulei, M.; Martin, J. D.; Corbett, J. D. *J. Solid State Chem.* **1996**, *125*, 249.

10.1021/ic990692w CCC: $19.00
Published on Web 12/16/1999

$Y_{16}Br_{24}Ir$, $Y_{20}Br_{36}Ir_4$,[12] and the cation-deficient $Sc_{19}Br_{28}Z_4$, Z = Mn, Fe, Ru, and Os.[13]

In the present investigation, we explored the stabilization of lanthanum bromide cluster phases through encapsulation of a variety of transition metal atoms such as Fe, Ru, and Os. Among these, only Os led to the observation and characterization of a new phase, $La_{48}Br_{81}Os_8$, with discrete clusters, but in a large superstructure that is distinctly different from that formed by the close R neighbor, $Pr_6Br_{10}Os$.[9] The present report describes its crystal structure and bonding.

Experimental Section

Syntheses. The general reaction techniques in welded $^3/_8$-in. diameter Nb tubing, the use of Guinier powder photography for both phase identification and approximate yield estimates, and the crystallographic characterization means have been described before.[7,10] All reactants and products were handled only in N_2-filled gloveboxes (H_2O < 0.1 ppm vol). The reagents La metal (Ames Lab), sublimed $LaBr_3$ (prepared from the elements), and Os powder (Alfa, 99.95% metal basis) were utilized on 200−300 mg reaction scales. Initial reactions that yielded the new phase had overall stoichiometric proportions between 6:6:1 and 6:9:3 (La:Br:Os) that had been heated at ~900−950 °C for 14 days, followed by cooling in the furnace. The products were, e.g. ~60% black crystalline $La_{48}Br_{81}Os_8$ and ~40% of LaOBr from the 6:9:1 starting composition. (The latter must have arisen from H_2O in the $LaBr_3$ or from the SiO_2 jacket or because of O in the metal.) A later reaction with the stoichiometric target $La_{48}Br_{81}Os_8$ heated at 900 °C for 6 days gave a ≥90% yield with only LaOBr as a discernible impurity. Interstitial candidates Mn, Fe, Co, Ru, and Ir did not give this phase.

X-ray Studies. An Enraf-Nonius (FR-552) Guinier camera was used to gain phase identification and refined lattice constants. Protection of the samples between layers of cellophane tape has been described earlier.[14] Powdered standard silicon (NIST) was included with each sample in order to provide an internal calibrant. Lattice constants were then obtained by standard least-squares refinement of measured and indexed reflections in each pattern. However, the sensitivity and resolution of this method yielded only smaller pseudotetragonal subcell parameters, $a' = b' = 8.2999(6)$ Å and $c' = 15.489(1)$ Å. The correct monoclinic supercell ($b = 2\sqrt{2}a' \cong c$, $a = 2c'/\sin(110.701°)$) could be detected only through precession photographs of single crystals taken with very long exposure times (1−2 days). It is to be noted that a correct unit cell was never detected for several crystals via the automatic searching routine for a four-circle Rigaku diffractometer with a rotating-anode source, only cells that were half or less of the correct cell. Since the *b* and *c* axes are similar ($\Delta \simeq 0.3\%$), a *b*- and *c*-axis exchange twinning is also possible.[15] Even a Bruker diffractometer with a charge-coupled detector (CCD) gave confusing cells (parameters) depending on the sample, between a larger primitive or a *B*-centered orthorhombic cell with the same cell parameters. The latter can be transformed to the correct primitive monoclinic cell reported in this work ($a = 33.076(5) = 30.941/\sin(110.701)$ Å, $b = 23.466(3)$ Å, $c = 23.537(2)$ Å and $\beta = 110.701(4)°$). These were refined from a set of ~6000 strong reflections collected from a single crystal that was not twinned.

Diffraction data were collected at room temperature on a Siemens (Bruker) SMART Platform diffractometer with a CCD detector over more than a hemisphere of reciprocal space ($2\theta < 55°$) from a 0.2 mm × 0.2 mm × 0.1 mm crystal sealed in a thin-walled capillary. A total of 187 279 reflections were measured. The SMART software was used for data acquisition, and SAINT, for data extraction.[16] From the cell parameters and angles, two Bravais lattices were possible: the above *B*-centered orthorhombic cell and its exact transformation into the primitive monoclinic cell with half the volume. The two cells resulted in almost the same crystal structure as far as the La_6Os clusters were concerned. However, the orthorhombic cell yielded some nonsensible bromine positions that were too close (<2 Å) to each other. These bromines were related to each other by false 2-fold or mirror symmetries along *c*-axis that the monoclinic cell does not have. The monoclinic cell finally assigned resulted in no such problem.

Table 1. Data Collection and Refinement Parameters for $La_{48}Br_{81}Os_8$

empirical formula	$La_{48}Br_{81}Os_8$
fw	14661.3
cryst system, space group, *Z*	monoclinic, $P2_1/c$ (No.14), 4
lattice consts (Å, Å^3, deg)[a]	$a = 33.076(5)$, $b = 23.466(3)$, $c = 23.537(3)$, $\beta = 110.701(4)$, $V = 17089(7)$
d_{calc} (g/cm^3)	5.70
μ(Mo Kα) (cm^{-1})	364.7
R, wR2,[b] all data (%)	16.94, 8.34
R, R_w,[b] $I > 3\sigma(I)$ (%)	3.75, 6.37

[a] Refined from ~6000 reflections in single crystal data set, $\lambda = 0.710\ 69$ Å, 23 °C. [b] $R = \sum||F_o| - |F_c||/\sum|F_o|$; $R_w = [\sum w(|F_o| - |F_c|)^2/\sum w(F_o)^2]^{1/2}$; $w = \sigma_F^{-2}$. $wR2 = [\sum w(|F_o|^2 - |F_c|^2)^2/\sum w(|F_o|^2)^2]^{1/2}$; $w = 1/(\sigma_F^2)^2$.

The data were first absorption-corrected with the aid of SADABS.[16] The absence conditions suggested a possible unique centric space group $P2_1/c$ (No.14), which gave 39231 averaged data with Friedel pairs merged ($R_{int} = 4.9\%$). Direct methods[17] yielded most metal positions. It must be emphasized that Fourier refinements[18] were used for the positional parameters because of disastrous coupling that occurred during least-squares refinements. The latter approach was at first employed only for isotropic temperature factors with appropriate shift-limiting restraints for all atoms.[19] After all 138 atoms had been found, several such cycles of combined Fourier and least-squares refinements against F^2 with all unique data were followed by a full least-squares refinements of both positional and thermal parameters with shift-limiting restraints. Application of DIFABS[20] to the model after isotropic refinement improved the absorption correction, as it provided more nearly spherical thermal ellipsoids. The final residuals after converged anisotropic refinement of all 138 atoms with 1238 variables were R(*F*)/wR2 = 16.94/8.34% for all 39 231 reflections, and $R(F)/R_w = 3.75/6.37\%$ for 6984 reflections with $I > 3\sigma(I)$. The largest residual peaks in a ΔF map were ±~2.1 e$^-$/Å^3, 0.8 Å from Os2 and 1.99 Å from Br71, respectively. Since the data set contained so many weak superstructure reflections, the residual R values were naturally larger. Some data collection and refinement parameters are given in Table 1, while more details are contained in the Supporting Information (Table S1). Because of their sizes, lists of the final atom coordinates, isotropic and anisotropic temperature factors, and their standard deviations are in Tables S2 and S3. Some important La−Br distances are in Table 2, while the complete interatomic distance list and some angles appear in Table S4. These and the F_o/F_c listing are available from J.D.C.

The Guinier powder pattern calculated for the refined structural model agreed very well with that observed for the bulk product. However, intensities calculated for all superstructure reflections are too small to be observed in Guinier patterns under our experimental conditions, even at low angles. But the more intense parts of the pattern are still sufficiently different that the superstructure would not be mistaken as that of a simpler $R_6X_{10}Z$ compound.

Results and Discussion

The Structure. Explorations in reduced lanthanum bromide systems with diverse transition metals as potential interstitials have produced only this monoclinic $La_{48}Br_{81}Os_8$, cluster phase,

(12) Steinwand, S. J.; Corbett, J. D. *Inorg. Chem.* **1996**, *35*, 7056.
(13) Steinwand, S. J.; Corbett, J. D.; Martin, J. D. *Inorg. Chem.* **1997**, *36*, 6, 6413.
(14) Daake, R. L.; Corbett, J. D. *Inorg. Chem.* **1978**, *17*, 1192.
(15) Pratt, C. S.; Coyle, B. A.; Ibers, J. A. *J. Chem. Soc. A* **1971**, 2146.
(16) SMART, SAINT V-4, SADABS Programs; Bruker Analytical X-ray Systems Inc.: Madison, WI, 1996.
(17) Sheldrick, G. M. *SHELXS-86*; Universität Göttingen: Göttingen, Germany, 1986.
(18) Watkin, D. J.; Prout, C. K.; Carruthers, J. R.; Betteridge, P. W. *CRYSTALS*, Issue 10; Chemical Crystallography Laboratory, University of Oxford: Oxford, U.K., 1996.
(19) Watkin, D. J. *Acta Crystallogr.* **1994**, *A50*, 41.
(20) Walker, N.; Stuart, D. *Acta Crystallogr.* **1983**, *A39*, 158.

Table 2. Some Important Distances (Å) in $La_{48}Br_{81}Os_8$

Os1−La3	2.623(2)	La1−Br38	3.037(5)	La10−Br13	3.149(4)	La20−Br52	3.105(4)	La30−Br69	3.166(5)	La40−Br10	3.084(4)
Os1−La2	2.675(2)	La1−Br62	3.105(4)	La10−Br17	3.222(4)	La20−Br78	3.200(5)	La30−Br31	3.202(5)	La40−Br1	3.135(4)
Os1−La5	2.947(2)	La1−Br21	3.120(4)	La10−Br17	3.441(4)	La20−Br22	3.223(4)	La30−Br9	3.296(4)	La40−Br66	3.301(4)
Os1−La6	2.971(2)	La1−Br23	3.395(4)	La11−Br50	3.007(4)	La20−Br65	3.224(4)	La30−Br1	3.370(5)	La40−Br72	3.442(4)
Os1−La1	2.998(3)	La1−Br28	3.450(5)	La11−Br3	3.030(4)	La20−Br18	3.604(5)	La31−Br42	3.010(4)	La41−Br48	3.091(4)
Os1−La4	3.006(2)	La2−Br19	3.061(4)	La11−Br4	3.078(4)	La21−Br52	3.032(5)	La31−Br67	3.025(5)	La41−Br10	3.143(4)
Os2−La11	2.641(2)	La2−Br61	3.115(5)	La11−Br26	3.121(5)	La21−Br11	3.093(5)	La31−Br75	3.027(5)	La41−Br37	3.213(4)
Os2−La12	2.666(2)	La2−Br12	3.137(4)	La11−Br25	3.204(4)	La21−Br81	3.095(5)	La31−Br6	3.144(4)	La41−Br7	3.226(5)
Os2−La10	2.966(3)	La2−Br24	3.139(4)	La12−Br18	3.073(5)	La21−Br35	3.150(4)	La31−Br20	3.383(5)	La41−Br66	3.228(5)
Os2−La7	2.985(2)	La2−Br73	3.233(5)	La12−Br57	3.106(4)	La21−Br12	3.165(4)	La31−Br58	3.602(5)	La41−Br49	3.389(4)
Os2−La8	2.994(2)	La2−Br77	3.320(4)	La12−Br54	3.133(4)	La22−Br58	2.976(5)	La32−Br33	2.982(4)	La42−Br46	3.065(5)
Os2−La9	3.000(3)	La3−Br74	3.053(5)	La12−Br65	3.263(4)	La22−Br81	3.053(5)	La32−Br67	3.076(5)	La42−Br53	3.151(5)
Os3−La14	2.639(2)	La3−Br2	3.054(4)	La12−Br79	3.272(4)	La22−Br47	3.129(5)	La32−Br13	3.089(4)	La42−Br30	3.171(4)
Os3−La16	2.647(2)	La3−Br16	3.118(4)	La12−Br76	3.351(5)	La22−Br22	3.204(5)	La32−Br3	3.157(4)	La42−Br1	3.243(5)
Os3−La13	2.912(3)	La3−Br5	3.125(4)	La13−Br71	3.018(4)	La22−Br55	3.210(4)	La32−Br54	3.164(4)	La42−Br43	3.268(4)
Os3−La15	2.920(3)	La3−Br21	3.160(4)	La13−Br46	3.049(4)	La23−Br36	3.001(5)	La32−Br4	3.245(4)	La42−Br34	3.316(4)
Os3−La17	2.987(2)	La4−Br24	2.987(4)	La13−Br55	3.079(4)	La23−Br11	3.064(5)	La33−Br45	3.029(4)	La42−Br55	3.608(4)
Os3−La18	3.004(2)	La4−Br2	3.097(4)	La13−Br22	3.154(4)	La23−Br47	3.067(4)	La33−Br17	3.045(4)	La43−Br68	2.966(4)
Os4−La21	2.626(3)	La4−Br15	3.101(4)	La13−Br75	3.183(5)	La23−Br69	3.122(5)	La33−Br51	3.105(5)	La43−Br64	3.100(4)
Os4−La19	2.658(3)	La4−Br62	3.139(5)	La13−Br79	3.328(4)	La23−Br38	3.243(5)	La33−Br48	3.279(4)	La43−Br15	3.131(4)
Os4−La24	2.934(3)	La4−Br63	3.277(4)	La14−Br55	3.028(4)	La24−Br78	3.020(5)	La33−Br13	3.305(4)	La43−Br19	3.154(4)
Os4−La23	2.962(3)	La4−Br44	3.491(5)	La14−Br44	3.072(4)	La24−Br35	3.027(5)	La33−Br40	3.452(4)	La43−Br2	3.169(4)
Os4−La22	2.970(2)	La5−Br12	3.018(4)	La14−Br63	3.097(4)	La24−Br49	3.151(4)	La34−Br42	3.016(4)	La43−Br5	3.235(4)
Os4−La20	3.002(3)	La5−Br72	3.103(4)	La14−Br64	3.196(4)	La24−Br31	3.391(5)	La34−Br45	3.058(4)	La44−Br68	3.039(5)
Os5−La28	2.651(2)	La5−Br5	3.173(4)	La14−Br53	3.237(4)	La25−Br16	3.048(4)	La34−Br33	3.091(5)	La44−Br23	3.120(4)
Os5−La25	2.652(2)	La5−Br15	3.196(4)	La15−Br56	3.054(4)	La25−Br49	3.080(4)	La34−Br78	3.159(4)	La44−Br15	3.144(4)
Os5−La30	2.941(2)	La5−Br28	3.320(4)	La15−Br63	3.078(4)	La25−Br69	3.136(4)	La34−Br26	3.238(5)	La44−Br81	3.224(4)
Os5−La27	2.952(3)	La5−Br23	3.444(4)	La15−Br37	3.082(5)	La25−Br10	3.188(4)	La35−Br76	2.980(5)	La44−Br34	3.279(4)
Os5−La29	2.964(2)	La6−Br19	3.059(4)	La15−Br77	3.173(4)	La25−Br41	3.201(4)	La35−Br51	3.067(4)	La45−Br23	3.018(4)
Os5−La26	2.995(3)	La6−Br38	3.067(5)	La15−Br39	3.236(4)	La25−Br60	3.227(4)	La35−Br8	3.094(4)	La45−Br64	3.069(4)
Os6−La36	2.648(3)	La6−Br72	3.117(4)	La15−Br35	3.250(5)	La26−Br16	3.025(4)	La35−Br3	3.179(4)	La45−Br34	3.087(4)
Os6−La34	2.660(3)	La6−Br74	3.123(4)	La16−Br70	3.101(4)	La26−Br47	3.065(4)	La35−Br26	3.301(5)	La45−Br61	3.177(4)
Os6−La35	2.921(3)	La6−Br60	3.224(4)	La16−Br71	3.118(4)	La26−Br1	3.086(4)	La36−Br75	3.085(5)	La45−Br43	3.203(4)
Os6−La32	2.954(2)	La6−Br29	3.354(4)	La16−Br37	3.126(4)	La26−Br30	3.116(4)	La36−Br17	3.095(4)	La45−Br5	3.203(4)
Os6−La33	2.968(2)	La7−Br50	3.038(4)	La16−Br59	3.151(4)	La26−Br68	3.239(4)	La36−Br76	3.134(5)	La46−Br41	2.995(4)
Os6−La31	3.051(3)	La7−Br54	3.045(5)	La16−Br33	3.203(4)	La26−Br60	3.257(4)	La36−Br4	3.257(4)	La46−Br28	3.046(4)
Os7−La37	2.614(2)	La7−Br20	3.148(5)	La16−Br79	3.256(4)	La26−Br34	3.537(4)	La36−Br32	3.302(4)	La46−Br39	3.099(4)
Os7−La40	2.676(2)	La7−Br80	3.217(4)	La17−Br77	3.020(5)	La27−Br25	2.952(4)	La37−Br14	3.001(4)	La46−Br73	3.126(5)
Os7−La41	2.975(2)	La7−Br40	3.224(5)	La17−Br79	3.028(4)	La27−Br49	3.071(4)	La37−Br48	3.060(4)	La46−Br11	3.233(4)
Os7−La38	3.008(3)	La7−Br51	3.360(4)	La17−Br14	3.231(4)	La27−Br7	3.097(4)	La37−Br32	3.061(4)	La46−Br21	3.254(4)
Os7−La39	3.013(3)	La8−Br65	2.981(4)	La17−Br59	3.234(5)	La27−Br31	3.118(4)	La37−Br46	3.079(4)	La47−Br29	3.026(4)
Os7−La42	3.056(2)	La8−Br3	3.087(4)	La17−Br52	3.340(4)	La27−Br45	3.264(4)	La37−Br57	3.214(4)	La47−Br39	3.034(5)
Os8−La44	2.640(2)	La8−Br13	3.185(4)	La17−Br53	3.363(5)	La28−Br30	3.044(4)	La38−Br32	2.972(4)	La47−Br73	3.178(5)
Os8−La44	2.640(2)	La8−Br71	3.208(4)	La18−Br44	3.021(5)	La28−Br27	3.068(4)	La38−Br9	2.976(4)	La47−Br2	3.215(4)
Os8−La45	2.956(2)	La8−Br8	3.270(5)	La18−Br70	3.041(4)	La28−Br25	3.081(4)	La38−Br27	3.078(4)	La47−Br62	3.219(4)
Os8−La45	2.956(2)	La8−Br70	3.434(4)	La18−Br56	3.075(5)	La28−Br80	3.084(4)	La38−Br7	3.134(4)	La47−Br21	3.278(4)
Os8−La43	2.958(2)	La9−Br18	2.972(4)	La18−Br22	3.241(5)	La28−Br67	3.221(4)	La38−Br40	3.306(4)	La48−Br29	3.089(5)
Os8−La43	2.958(2)	La9−Br20	3.056(5)	La18−Br52	3.456(4)	La28−Br58	3.537(5)	La39−Br56	3.054(4)	La48−Br28	3.117(4)
Os9−La48	2.779(2)	La9−Br8	3.118(4)	La18−Br14	3.488(4)	La29−Br80	3.081(5)	La39−Br66	3.070(4)	La48−Br41	3.155(4)
Os9−La48	2.779(2)	La9−Br26	3.236(4)	La19−Br36	3.053(4)	La29−Br60	3.081(4)	La39−Br43	3.081(4)	La48−Br39	3.191(4)
Os9−La47	2.927(2)	La9−Br42	3.389(5)	La19−Br6	3.088(5)	La29−Br10	3.241(4)	La39−Br14	3.111(4)	La48−Br66	3.223(4)
Os9−La47	2.927(2)	La9−Br42	3.443(5)	La19−Br58	3.100(4)	La29−Br36	3.270(4)	La39−Br53	3.225(4)	La48−Br72	3.408(4)
Os9−La46	2.965(2)	La10−Br57	3.056(4)	La19−Br78	3.191(5)	La29−Br9	3.305(4)	La39−Br24	3.262(4)		
Os9−La46	2.965(2)	La10−Br40	3.088(4)	La19−Br31	3.256(4)	La29−Br7	3.336(5)	La40−Br43	3.014(4)		
La1−Br61	2.963(4)	La10−Br4	3.092(4)	La20−Br59	3.087(4)	La30−Br27	3.075(5)	La40−Br9	3.051(4)		

a new and large structure type with isolated clusters. Even the common interstitials Fe and Ru gave no identifiable analogue of known Pr or Y bromides[9,12] or of lanthanum iodides La_3I_3Z (Z = Ru, Os, Ir, Pt),[21] La_4I_5Ru,[22] or the dimeric $La_{10}I_{15}Os_2$.[23]

The new structure is constructed essentially from distorted or modified La_6Br_{12}-type (edge-bridged) clusters centered by osmium, as already known in the compositionally related but much simpler $Pr_6Br_{10}Os$ clusters and, in fact, in most cluster halides. Figure 1 shows for later comparison and contrast one face of the unit cell of triclinic Pr_6Br_{10}(Os,Ru).[9] This contains two varieties of the intercluster bromine connectivities that customarily fill exo positions at metal vertexes. Horizontally, pairs of dual edge-bridging Br^{i-i} atoms connect the clusters into infinite chains, whereas complementary pairs of Br^{i-a}, Br^{a-i} interbridge clusters both vertically and in the third direction not shown. In contrast, Figure 2 shows in outline the usual La_6Os (tetragonally compressed) octahedra in $La_{48}Br_{81}Os_8$ in a view parallel to the unique *b* axis, with bromine atoms omitted for clarity. The structure can be considered to be built from CsCl-type stackings of four cluster layers along the *a* axis or, more exactly, along the [100] direction, with two orientations of the La_6Os octahedra. In the first layer (numbered from left to right), the approximate 4-fold axis of the compressed octahedra lies along $\vec{b}$, while in the second layer this runs along $\vec{c}$, and these repeat in the third and the fourth layers. Figure 3 shows that each layer consists of a tetragonally elongated CsCl-type arrangement viewed along [100], viz., a rough cube of eight

(21) Dorhout, P. K.; Payne, M. W.; Corbett, J. D. *Inorg. Chem.* **1991**, *30*, 4960.
(22) Payne, M. W.; Dorhout, P. K.; Corbett, J. D. *Inorg. Chem.* **1991**, *30*, 1467.
(23) Lulei, M.; Martin, J. D.; Hoistad, L. M.; Corbett, J. D. *J. Am. Chem. Soc.* **1997**, *119*, 513.

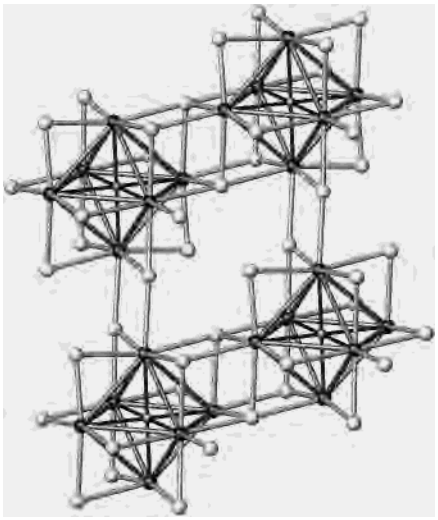

Figure 1. Structure of Pr_6Br_{10}(Os,Ru) viewed along $\vec{b}$. Pairs of dual edge-bridging Br^{i-i} atoms connect the clusters into infinite chains that run nearly horizontally, whereas complementary pairs of Br^{i-a}, Br^{a-i} interbridge clusters both vertically and in the third direction not shown. Inversion centers lie at the centers of the clusters and at the centers of all cell edges within the bridging arrays.

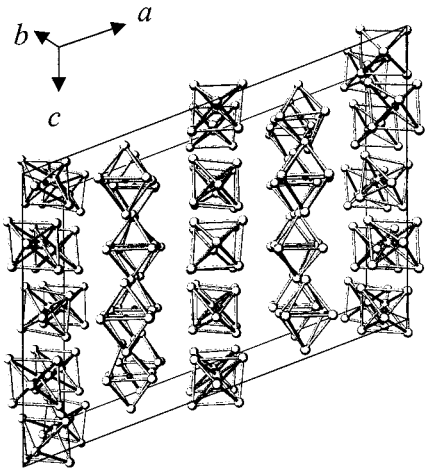

Figure 2. La_6Os octahedral cluster arrangements in the unit cell of $La_{48}Br_{81}Os_8$. Each octahedron is centered by a Os atom (black), while bromine atoms are not shown for clarity.

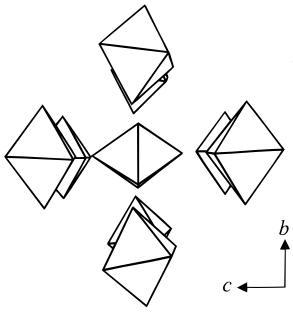

Figure 3. Elongated CsCl-type arrangement of nine La_6Os clusters shown as polyhedra. Cluster 5 is central. This arrangement can be considered as a smallest building unit in $La_{48}Br_{81}Os_8$.

La_6Os clusters centered by a ninth. The intralayer Os−Os distances are ∼8.3 Å, while those between the pseudoeclipsed (top and bottom) cluster layers are ∼15.5 Å. The cluster in the center is rotated by 90° from neighboring clusters to yield less steric hindrance. This quasi-tetragonal cluster unit forms a basic building unit for the whole structure, consistent with the strongest diffraction spots observed for the corresponding subcell. The unit cell contains 16 such groups in the superstructure.

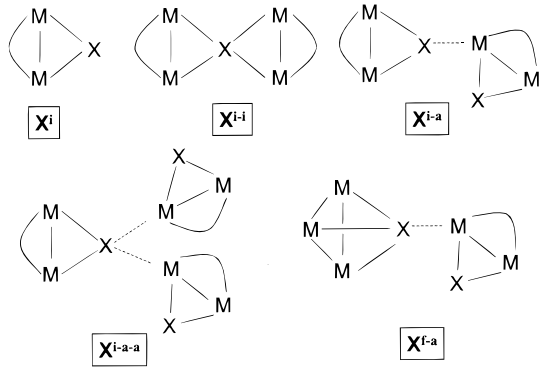

Figure 4. Various halide functions about clusters in $La_{48}Br_{81}Os_8$.

Bromine Functions. The ideal, or most common, octahedral metal cluster is enclosed by 12 inner edge-bridging (Br^i) plus six exo-bonding (or outer, Br^a) bromides at the vertexes that are commonly bifunctional and also inner atoms in neighboring clusters (Br^{a-i}). But in $La_{48}Br_{81}Os_8$, this prototype connectivity is much modified and distorted, and several other types of bromine functions appear, generally featuring a greater number of bonds per bromine to go along with the low Br:La ratio. The present structure contains some vertexes with (a) two Br^a, (b) double-edge-bridging Br^{i-i}, (c) a new face-capping function (Br^{f-a}) for a Br^a on another cluster, and (d) a rarely known example of Br^i that is also exo to vertexes in two other clusters (Br^{i-a-a}).[11] The five types Br^i, Br^{i-i}, Br^{i-a}, Br^{i-a-a}, and Br^{f-a} types are illustrated in Figure 4 in this order for halide (X) in general where

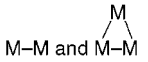

represent edges and faces of the metal clusters. Sterically, the 12 X^i atoms in 6−12 clusters generally provide a tightly packed array, and the principal space for additional bonding occurs in the reduced hemispheres that lie outward from each vertex. (We note that X^{f-a} functionality is already known in some more open, elongated trigonal bipyramidal cluster halides such as $La_5(C_2)Br_9$.[24])

There are nine independent Os atoms and the corresponding number of pseudooctahedral cluster types in $La_{48}Br_{81}Os_8$, two with a lower multiplicity (8, 9) and one that is more distorted (7). Even though the octahedra themselves are not easily distinguished from one other, they are readily classified according to the surrounding bromine functions and connectivity, as is summarized in Table 3. Clusters 1 and 2 have 12 inner bromines about each that cover the 12 edges in one manner or another. Note that the other seven clusters are all different in their closely bonded bromines, and these include three (4, 6, 7) with only 10 or 11 nearest neighbors and five that have one or two of the unusual face-capping "inner" bromines (Br^{f-a}). In the same sense, the wide variety of cluster halides known to date nearly always have just six halogens bonded exo at the six vertexes of the nominal octahedra. The complexity (and perversity) of the present structure is further emphasized by the tabulation of *a* functions (right-hand block) in Table 3, where different clusters are shown to have 7−10 (mainly 8) exo-bonded Br^{a-} in diverse arrangements. Overall, the clusters show a range from 18 (cluster 4) to 22 (cluster 8) total bromines within

(24) Heuer, T.; Steffan, F.; Meyer, G. *Eur. J. Solid State Inorg. Chem.* **1996**, *33*, 265.

Table 3. Number of Bromine Atoms about Each Cluster in $La_{48}Br_{81}Os_8$, Sorted by Cluster Type and Bromine Function[a]

	functions[c]									
cluster no.[b]	i	i−i	i−a	i−a−a	f−a	a−i	a−a−i	a−f	tot. Br/cluster	formula, Br/La_6Os[d]
1 (1−6)	2	3	6	1		6	0	1	19	10.25
2 (7−12)	2	3	6	1		7	0	1	20	10.58
3 (13−18)	2	2	7	0	1	7	0	1	20	11.00
4 (19−24)	1	1	7	0	1	8	0		18	9.58
5 (25−30)		3	8	0	1	6	2		20	10.08
6 (31−36)		3	8	0		6	2	1	20	9.58
7 (37−42)		4	4	1	2	8			19	9.33
8 (43−45)	2	4	6	0		6	2	2	22	11.00
9 (46−48)		2	8	0	2	4	2	2	20	10.17
fraction	1	$^2/_4$	$^2/_3$	$^2/_4$	$^3/_4$	$^1/_3$	$^1/_4$	$^1/_4$		
tot[e]	8	22	53	3	6	53	6	6		81

[a] Typical d(La−Br) ranges are 2.95−3.30 Å for edge-bridging (i, i−a) or face-capping (f) and 3.09−3.39 Å for exo-bonding (a−) functions. [b] Each cluster is identified by the number of the centered osmium, Table 2. The lanthanum atom numbers in each are given in parentheses. [c] i inner, edge bridging; a, to vertex; f, face-capping. [d] Each cluster can be represented by a composition, splitting each bromine according to the number of La to which it is bonded, not distinguishing i from a. For example, cluster 1 is $La_6(Os)(Br^i)_2(Br^{i-i})_{3(2/4)}(Br^{i-a})_{6(2/3)}(Br^{i-a-a})_{1(2/4)}(Br^{a-i})_{6(1/3)}(Br^{a-f})_{1/4} = La_6(Os)Br_{10.25}$ (last column). [e] Clusters 8 and 9 have half the multiplicity of the other clusters. These totals are per formula unit.

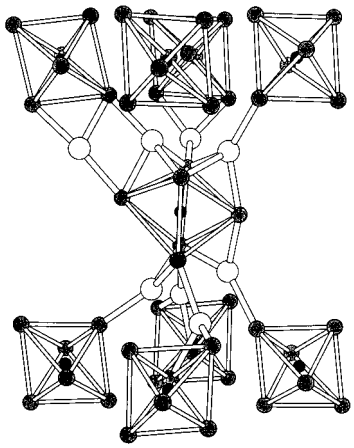

Figure 5. Part of the environment about the most distorted cluster 7 (center) within the layer of interbridged clusters. Distinctive features include two Br^{f-a} at top and one unbridged metal edge (lower left front).

what we judge to be bonding distances (Table 3, footnote *a*) where 18 is "normal" $[(X^i)_{12}(X^a)_6]$. The conformations about most lanthanum and bromine atoms are fairly regular and obvious on inspection of distance tables. On the other hand, the particularly distorted cluster 7 in the center of Figure 5 has two Br^{f-a} functions. In addition, one edge (La38−La42) is elongated 0.5 Å beyond the normal range (lower left front) and remains unbridged, and all but two metal atoms in the cluster have two Br^a neighbors.

If the bromines are assigned equally among the lanthanum atoms to which each is bonded, that is, disregarding i, a, and f differences, we can gain an approximate composition for each cluster. For example, cluster 1 is in this sense $La_6(Os)(Br^i)_2(Br^{i-i})_{3(2/4)}(Br^{i-a})_{6(2/3)}(Br^{i-a-a})_{1(2/4)}(Br^{a-i})_{6(1/3)}(Br^{a-f})_{1/4}$, or $La_6(Os)Br_{10.25}$, and the others are as given in the last column in Table 3. The average cluster in the compound is $La_6(Os)Br_{10.125}$, and the average cluster-based electron count is $[(48(3) - 81(1) + 8(8)]/8 = 15.875 \sim 16$. Our crude assignment does not allow anything more to be said about the actual electron distributions, although different and significant La−Br bond polarities are expected.

Cluster Distortions. Eighteen skeletal electrons are optimal for nominally octahedral 6−12 type clusters that are centered by transition metal elements, corresponding to a skeletal electron distribution into the R−Z bonding $a_{1g}^2t_{2g}^6$, the nominally nonbonding e_g^4 on Z, and the R−R bonding t_{1u}^6 HOMO in terms of octahedral representations.[25] The present complex phase is

Table 4. Degree of Tetragonal Compression of the Clusters in $La_{48}Br_{81}Os_8$ As Measured by d(Os−La) Differences (Å)

cluster type	Δd(odd axis)[a]	$\bar{d}$(La−Os)	compression axis (La)
1	0.332	2.870	2, 3
2	0.332	2.875	11, 12
3	0.313	2.852	14, 16
4	0.325	2.859	19, 21
5	0.311	2.859	25, 28
6	0.320	2.867	34, 36
7	0.368	2.890	37, 40
8[b]	0.317	2.851	44, 44
9[b]	0.167	2.890	48, 48

[a] The difference between the average of four longer and two shorter d(Os−La). [b] Centric.

short only one electron per formula unit of an average (ideal) t_{1u}^4-type HOMO configuration for all nine cluster types. The effect of a ground-state deficiency t_{1u}^4 is well-known to afford general tetragonal compressions of 16-electron clusters, as observed in $Y_6I_{10}Ru$ ($\Delta\bar{d}$(R−Z) = 0.21 Å),[8] $Pr_6Br_{10}Ru$ (0.28 Å, vertical in Figure 1),[9] $K_2La_6I_{10}Os$ (0.25 Å),[26] and less in $Y_6I_{10}Os$ (0.18 Å).[7] MO calculations on $Y_6I_{10}Ru$ indicated that interactions between 4d orbitals on the Y atoms cause a splitting of the nominal t_{1u}^4 HOMO into e_u^4 below b_{2g}.[8] Very similar distortions are found in $La_{48}Br_{81}Os_8$ in general, as summarized in Table 4. The first eight clusters show 0.31−0.37 Å decreases in axial d(La−Os) (i.e., ∼0.67 Å apex-to-apex), while cluster 9 changes only about half as much. It may be that two extra holes lie in a nominal t_{1u}^2 (→ e_u^2) on the least compressed (and half as frequent) cluster 9, but this is really not clear. Five of the clusters contain one or two anomalous Br^f face-capping functions (Table 3). Although it is well-known that capping all faces changes electronic requirements of clusters considerably,[27] we have here five examples of only partial changes toward that limit, most containing no symmetry elements. Thus calculations to pinpoint the possibly single electron hole per f.u. seem relatively profitless. The widespread tetragonal compressions of the clusters still seem to be the best hint of *relatively* simple effects. The same cautions apply as much or more to possible magnetic susceptibility properties, where even unique and nearly ideal geometries do not always give a simple result (summarized in ref 28).

(25) Hughbanks, T.; Rosenthal, G.; Corbett, J. D. *J. Am. Chem. Soc.* **1988**, *110*, 1511.
(26) Uma, S.; Corbett, J. D. *Inorg. Chem.* **1998**, *37*, 1944.
(27) Hughbanks, T. R. *Prog. Solid State Chem.* **1989**, *19*, 329.

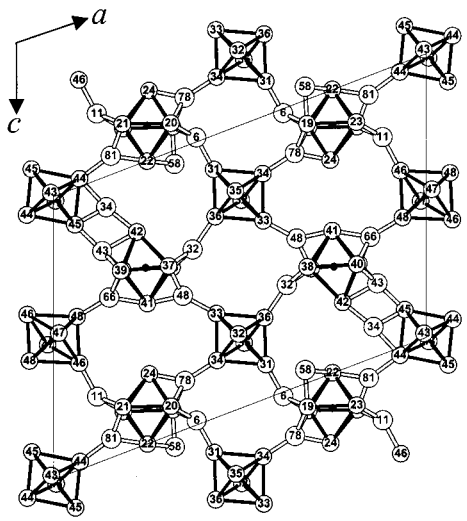

Figure 6. [010] view of the $a-c$ plane in $La_{48}Br_{81}Os_8$ at $y \approx 0$ with La shaded and Os black. La−La and La−Br bonds are shown as filled and shaded, respectively. All the bromines bridging clusters in this plane are shown.

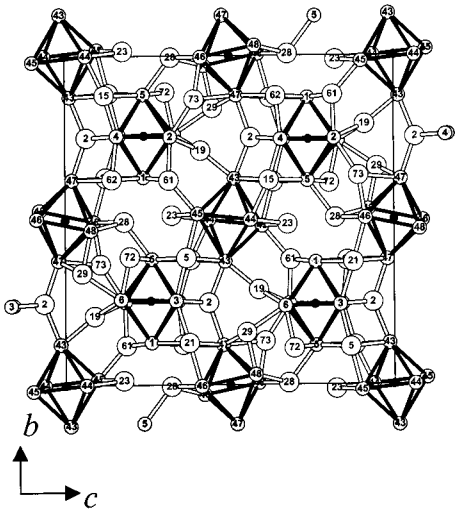

Figure 7. [100] view of the $b-c$ plane in $La_{48}Br_{81}Os_8$ at $x \approx 0$.

The Superstructure. As can be expected from the variety of functions listed in Table 3, the complete structure of $La_{48}Br_{81}Os_8$ is very complicated, and we will show only some exemplary sections for simplicity. Figure 6 shows an [010] section ($a-c$ plane) around the clusters at $y = 0$ with only the innerbridging or interconnecting bromines in the plane shown for clarity. Examples of i (Br58), i−a (Br6,11,32,34,48,81) and f−a (Br43,66,78, in projection) functions are visible. Figure 7 shows the bromine-richer connectivity in the perpendicular $b-c$ plane [100] for clusters centered around $x = 0$. This shows examples of i−i (5, 15, 21), and i−a−a (2) connections as well. Several metal vertices are also seen to have more than one exo-bonded bromine, e.g., La43 and La47. This view contains a number of Br^{i-i} functions characteristic of $Pr_6Br_{10}Os$ (Figure 1) but without much order.

The 2-D bromine connectivity in the $b-c$ plane (Figure 7) combined with a perpendicular one such as $a-c$ (Figure 6) gives a start at the network structure, but it would be very difficult to show all such connectivities by means of figures. In Figure 8 we show only the neighboring (upper and lower) [100] sections

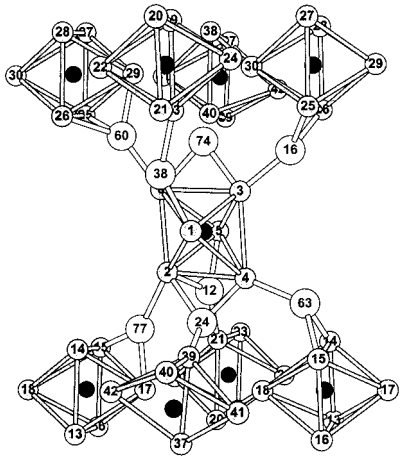

Figure 8. Interlayer bromine bridging function around cluster 1. Bromines involved in intralayer connectivity (Figure 7) are not shown for clarity.

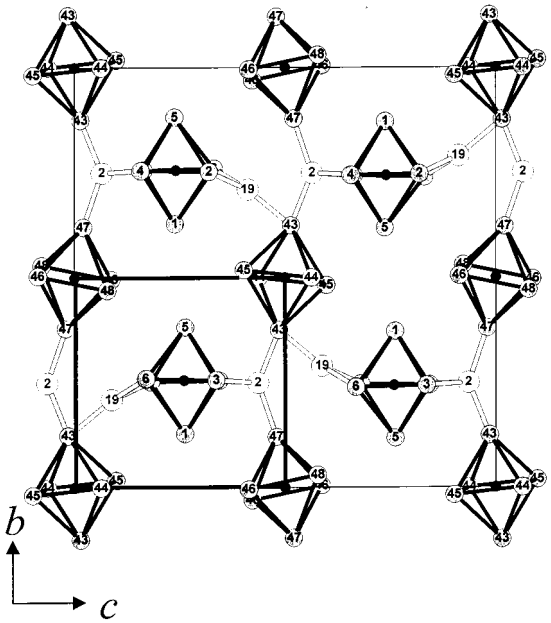

Figure 9. Zigzag ordering of clusters and bromine functions in the $b-c$ plane at $x \approx 0$ (Figure 7) with only Br2 and Br19 are shown for clarity. A possible subcell is shown with thicker lines.

that lie around cluster 1. For clarity, the view is along [0$\bar{1}$0], ~90° from that of Figure 7. This also means that the bromines shown here are entirely new and connect clusters *inter*plane. We can also see the clear f−a role of Br60 on cluster 5.

Although reasons why $La_{48}Br_{81}Os_8$ achieves its particular and rather complex superstructure relative to the neighboring $Pr_6Br_{10}Os$ (Figure 1) seem unclear, it is evident that the increased numbers of the polar La−Br interactions are a major driving force. Thus each cluster (but number 4) has an excess (1−4) of bonded bromines compared with the normal 18. This generates, and the structure allows, more crowded closed-shell contacts between bromines, new bromine functions, and complex and presumably delicate orderings of cluster orientations and bromine connectivities. Electronic contributions among the various distorted clusters are not clear beyond the rather uniform tetragonal compressions. Rather than showing more details of all of the structural motifs, we will show two relatively clear characteristics of the superstructure. Figure 9 is a repeat of Figure 7 with all bromines but Br2 and 19 eliminated. An alternate subcell (heavier lines) is also drawn. Cluster orientation

(28) Uma, S.; Martin, J. D.; Corbett, J. D. *Inorg. Chem.* **1999**, *38*, 3825.

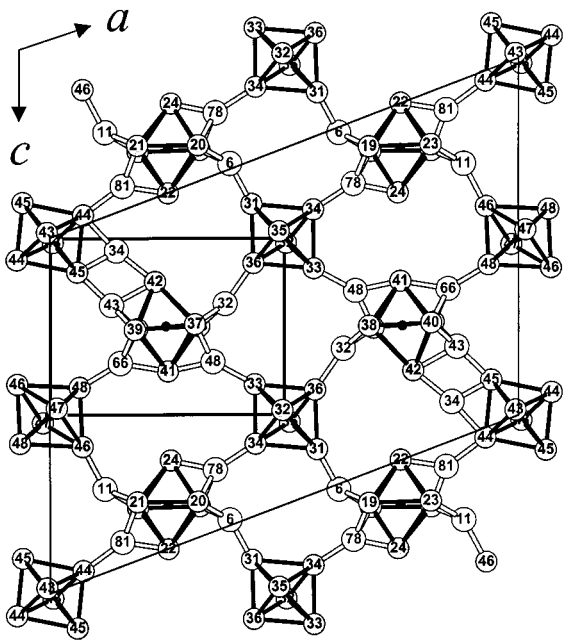

Figure 10. Ordering of clusters in the $a-c$ plane in $La_{48}Br_{81}Os_8$ at $y \approx 0$ (as in Figure 6) but only intralayer bromines shown for clarity. A possible subcell is marked with thicker lines.

on the left half of this figure is very similar to that on the right, suggesting a $c/2$ pseudocell. The centered clusters type 1 in the bottom and top halves (along 0, y, $^1/_4$, etc.) are rotated so that the Br2 and Br19 functions are ordered and alternate along b. In an ideal subcell, these would be fixed, and Br19 would have i−a-a function as Br2 already does. However, this would put Br2 and Br19 too close to each other, much less than the observed 3.71 Å. This steric hindrance may be the reason for the observed variation in functions for Br2 and 19, the zigzag ordering of clusters, and the longer b axis. Ordering in the neighboring $b-c$ plane at $x = {}^1/_4$, $^3/_4$, however, is the other way round, consistent with the supercell formation along c.

The character of the supercell formation along a is rather subtle. Figure 10 shows the $a-c$ plane of Figure 6 again and a possible subcell. This view contains cluster types 4, 6, 7, 8 and 9, but it shows only Br^{i-a} or Br^{f} (43, 66, 78) to clusters 4 and 7, and Br^{a-i} or Br^{a-f} to clusters 6, 8, or 9. As before, clusters 4 and 7 alternate along c with rotation between adjoining columns. Alternatively, the last are also related to each other by inversion centers on the origin, faces, edges, and middle of the true cell. This doubles the cell along [001] but with an obtuse angle in a monoclinic cell.

The Bottom Line: Better Space Filling. The present complicated phase is clearly a novelty, and an important one it seems. Many isostructural pairs of compounds have been observed for cluster halides of La and Pr, La_2INi_2 and Pr_2INi_2,[29] La_3I_3Ru and Pr_3I_3Ru,[30] La_3I_3Os and Pr_3I_3Os,[21] La_4I_4Ru and Pr_4I_4Ru,[22] $La_{12}I_{17}Fe_2$[11] and $Pr_{12}I_{17}Fe_2$,[10] $CsLa_6I_{10}Fe$ and $CsPr_6I_{10}Fe$,[31] and $Cs_2La_{10}I_{17}Os_2$ and $Cs_2Pr_{10}I_{17}Os_2$.[23] No other superstructures have been noted, although certainly some may have remained as "unknown products", even in the Pr−Br−Os system. The above pairs of comparisons all exhibit small increases in cell volume from the Pr to the La member, 3.1−5.4% without exception, presumably because of larger size of La. But in the present case, no analogue of the triclinic $Pr_6Br_{10}Os$ ($Z = 1$) has been seen. Instead, the very slightly oxidized $La_6Br_{10.125}Os$ ($Z = 8{\cdot}4$) is favored in a large monoclinic structure but still one built of isolated clusters. A striking feature regarding its stability is the volume per cluster, which is 9.4% *less* than that of $Pr_6Br_{10}Os$ despite small opposing effects from atom size differences![32] Clearly we have stumbled on the rare favorable case in which just the right size proportions of all three elements and of their cluster units (and, possibly, unknown electronic effects of the distortions) allow favorable increases in R−X interactions. Strong, polar La−Br bonding must be a major part of the gain, and the increases in coordination numbers of each by the other express this. Five Br about each La vertex is the normal situation, but here 17 (of 48) La have six Br neighbors, and two La, only four Br. Correspondingly 20 of 81 Br have the expanded 4-fold bonding interactions with La (Table 3). The large cell represents the difficulty of achieving this in an efficient, periodic manner.

Matrix effects—important closed-shell repulsions between, mainly, halide anions plus any changes in R−R and R−Z distances with cluster distortion[33]—must be the effects that limit bonding here. These are expressed, in part, by particularly short d(Br−Br), of which there are three notable examples <3.4 Å: 3.393(6), 3.317(7), and 3.300(5) Å for d(Br39−41), d(Br42−42), and d(Br9−36), respectively. The first involves Br^{f-a} and Br^{i-a} on a common cluster, and the other two involve atom pairs that are both Br^{a} to a common La vertex. These are very short compared with the smallest distances in other cluster bromides, 3.452(4) Å in $Na_2Pr_4Br_9NO$, 3.408(2) Å in $Pr_8Br_{13}N_3O$ (both Pr^{III}),[34] and 3.451(3) Å in $K_4Nb_6Br_{18}$.[35]

Acknowledgment. We thank Ilia Guzei for provision of the Bruker CCD diffractometer in good operating condition. This research has been supported by the National Science Foundation, Solid State Chemistry, via Grants DMR-9207361, -9510278, and -9809850 and was carried out in the facilities of the Ames Laboratory, U.S. Department of Energy.

Supporting Information Available: Tables of crystallographic and refinement parameters, positional and thermal parameters (isotropic and anisotropic) for all atoms, all interatomic distances < 4.3 Å, and some angles. This information is available free of charge via the Internet at http://pubs.acs.org.

IC990692W

(29) Hong, S.-T.; Martin, J. D.; Corbett, J. D. *Inorg. Chem.* **1998**, *37*, 3385.
(30) Payne, M. W.; Dorhout, P. K.; Kim, S.-J.; Hughbanks, T.; Corbett, J. D. *Inorg. Chem.* **1992**, *31*, 1389.
(31) Lulei, M.; Corbett, J. D. *Z. Anorg. Allg. Chem.* **1996**, *622*, 1677.
(32) Biltz's volume estimate for La vs Pr, 0.4 cm^3 mol^{-1}, increases the volume contrast to 10.0%. The effect of an extra $^1/_8$ Br per cluster is negligible. Biltz, W. *Raumchemie der Festen Stoffe*; Leopold Voss: Leipzig, Germany, 1934; p 238.
(33) Corbett, J. D. *J. Solid State Chem.* **1981**, *37*, 335.
(34) Lulei, M.; Steinward, S. J.; Corbett, J. D. *Inorg. Chem.* **1995**, *34*, 2671.
(35) Ueno, F.; Simon, A. *Acta Crystallogr.* **1985**, *C41*, 308.